CHAPTER 2

THEORETICAL ASPECTS

This chapter deals with various theoretical models that have been used to explain the mechanisms of charge storage and charge transport in the nanocomposite systems investigated in the present thesis. Different parameters governing the charge storage performance of supercapacitors have been discussed. This is followed by the description of theories of various electrochemical methods employed for studying the electrochemical performance of supercapacitors. The models used for calculation of specific surface area, pore size, pore volume and surface energy have been discussed. Finally theories governing the interaction of swift heavy ions with solid target material have been explained briefly.

2.1 Models of electric double layer formation

The electric double layer (EDL) charge storage mechanism is based on the accumulation of charge carriers at the interface when a charged material is placed inside a liquid. The balancing counter charge of the liquid accumulates on the surface of the charged material in order to meet the electro-neutrality requirement. In EDL capacitors, the charged material represents the electrode and the liquid is the electrolyte. Upon applying an external potential to the electrode, a capacitance is developed at the electrode-electrolyte interface due to electrostatic accumulation of charges, which depends on the applied electrode-potential [123]. The schematic of charging and discharging processes in an EDL capacitor and their corresponding electric potential profiles are illustrated in Figures 2.1 (a) and (b). During charging, the electrons flow from the positive electrode to the negative electrode through an external circuit, while the electrolyte cations and anions accumulate on the negative and positive electrode, respectively. The accumulation of charges at both the electrode-electrolyte interfaces form two individual electric double layer capacitors in series, where the charges are separated by a few Å. The reverse processes occur during discharge. In the charged condition, there are two interfacial potential drops across each double layer capacitor. During discharge state, there is also a current-dependent ohmic IR drop in potential within the solution. There are no charge

transfer processes and exchange of ions involved in EDL charge storage, which implies that the concentration of electrolyte does not vary during charging and discharging.

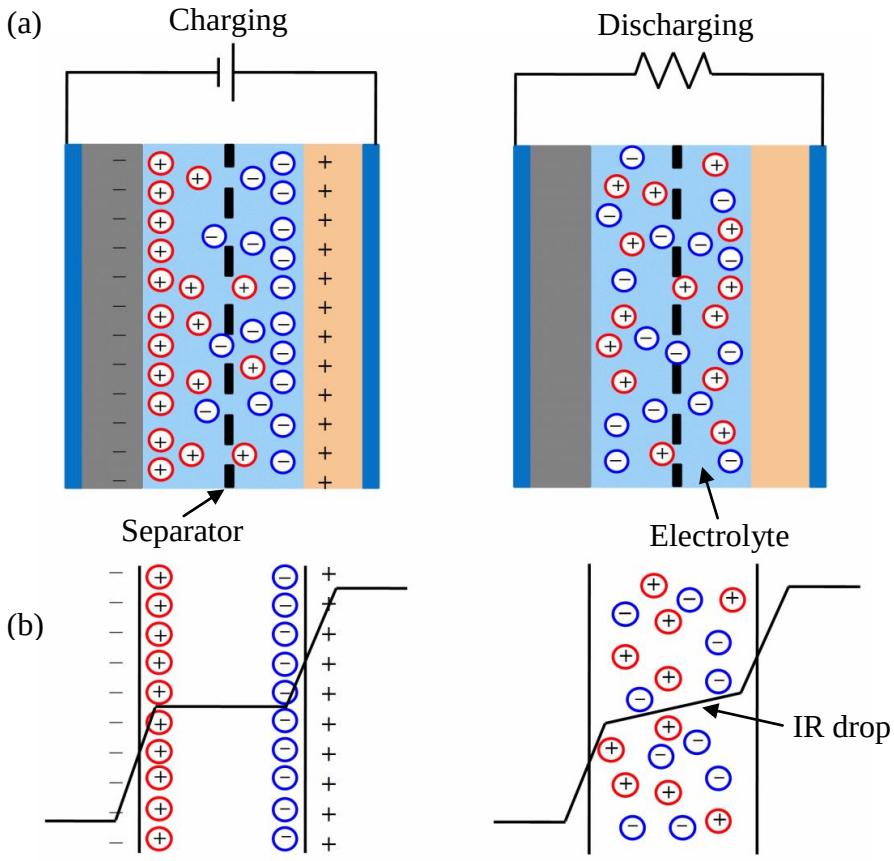

Figure 2.1: *Schematic of (a) charging and discharging processes in an EDL capacitor and (b) their corresponding electric potential profiles.*

The electrochemical processes during charging and discharging at the positive and negative electrode can be expressed as [214]:

$$E_P + A^- \rightarrow E_P^+//A^- + e^- \quad (charging) \tag{2.1}$$

$$E_P^+//A^- + e^- \rightarrow E_P + A^- \quad (discharging) \tag{2.2}$$

$$E_N + C^+ + e^- \rightarrow E_N^-//C^+ \quad (charging) \tag{2.3}$$

$$E_N^-//C^+ \rightarrow E_N + C^+ + e^- \quad (discharging) \tag{2.4}$$

where E_P is the positive electrode, E_N is the negative electrode, A^- is the anion, C^+ is the cation and // represents the electrode-electrolyte interface. The overall charging and discharging processes can be written as:

$$E_P + E_N + A^- + C^+ \rightarrow E_P^+//A^- + E_N^-//C^+ \quad (charging) \tag{2.5}$$

$$E_P^+//A^- + E_N^-//C^+ \rightarrow E_P + E_N + A^- + C^+ \quad (discharging) \tag{2.6}$$

Several models have been proposed to describe the spatial distribution of charges at the EDL interfaces, namely the Helmholtz model, the Gouy-Chapman model and the Stern model, which are described in the following sub-sections:

(i) Helmholtz model: The EDL theory was first described and modelled by von Helmholtz in 1853, which provides the simplest approximation of the potentiostatic behavior of electrode in solution [144]. This model states that an electrode immersed in an electrolyte forms a layer of opposite charges of ions at the electrode-electrolyte interface at a distance 'd' from its surface as shown in Figure 2.2 (a), where 'Ψ' is the potential developed at the interface and 'Ψ_0' is the electrode potential. The Helmholtz model is similar to that of a parallel-plate capacitor, which considers the formation of only a single rigid layer of electrolyte ions at the interface to neutralize the charges at the electrode surface. The capacitance given by the Helmholtz model is:

$$C_H = \frac{\varepsilon}{d_H} \tag{2.7}$$

where d_H is the thickness of the Helmholtz double layer and ε is the permittivity of the electrolyte. However, this model could not accurately determine the relation between capacitance and voltage as it did not consider the electrolyte resistance which can lead to a different charge distribution [215].

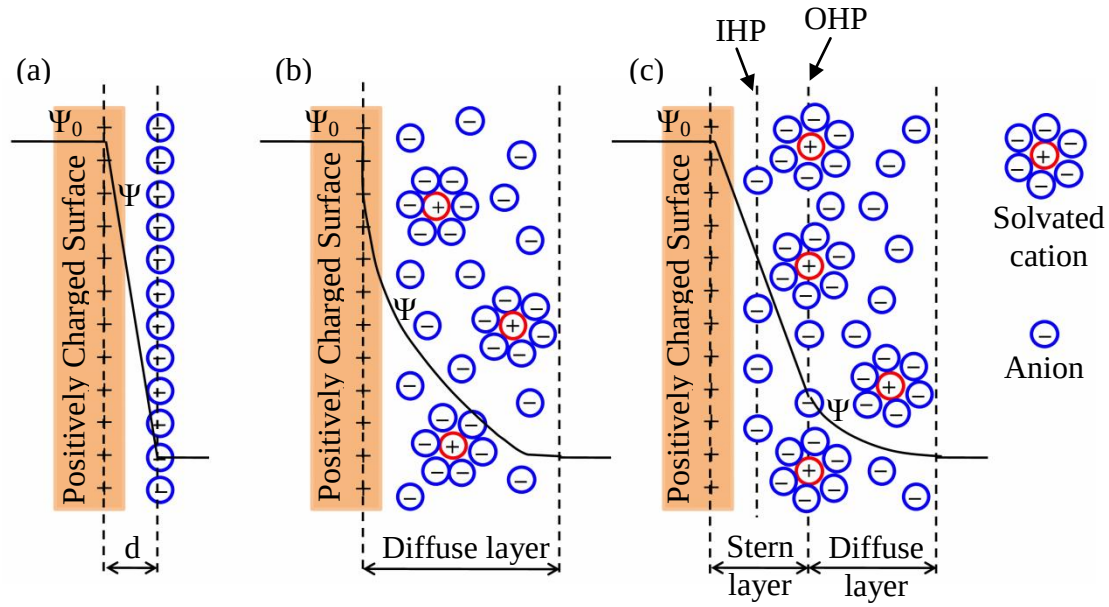

Figure 2.2: *EDL models, (a) Helmholtz model, (b) Gouy-Chapman model, and (c) Stern model.*

(ii) Gouy-Chapman model: The Helmholtz model was modified by Gouy [216] and Chapman [217] based on the consideration that ions in the electrolyte solution of the double layer does not remain static at the interface in a compact array, but are subjected to thermal fluctuation effects according to the Boltzmann principle. Gouy suggested that the electrolyte counterions conjugating to the electrode's surface charge are three-dimensional diffusely distributed population of cations and anions, which have an equal and opposite net charge density to the two-dimensional excess or deficit electronic charge on the metal surface. In this theory, the ions were considered to be point charges that tend to diffuse in the solution and the ion concentration near the surface follows the Boltzmann distribution as shown in Figure 2.2 (b). The thickness of the diffuse layer will be determined by the kinetic energy of the ions in the solution. The capacitance defined by the Gouy-Chapman model is referred to as the "diffuse" double-layer capacitance and is derived as:

$$C_{diff} = \frac{Q_{diff}}{\Psi_0} = \frac{(-\varepsilon k_B T)\frac{d\Psi}{dx}}{ze\Psi_0} = \frac{2\varepsilon k_B T}{ez\lambda_D \Psi_0} Sinh\left(\frac{ze\Psi_0}{2k_B T}\right) \quad (2.8)$$

where z is ionic valence, e is electronic charge, k_B is Boltzmann constant, T is temperature, λ_D is the thickness of the diffuse layer and ε is the electrolyte permittivity. If $\Psi << (2k_BT/ze)$ is satisfied, the diffuse capacitance is approximated as:

$$C_{diff} = \frac{\varepsilon}{\lambda_D} \quad (2.9)$$

However, the Gouy-Chapman model led to a failure due to an incorrect local field and potential profile at the electrode interface, which predicted a too-large EDL capacitance being defined as the rate of change of total ionic charge in the electrolyte solution with the change in potential difference across the electrode-electrolyte interface. This problem arises because the capacitance of both the double layer arrays of charges increases with a decrease in their separation distance giving rise to very large capacitance values in case of point charge ions accumulated on the electrode surface.

(iii) Stern model: The shortcomings of the Gouy-Chapman model of overestimation of the EDL capacitance was resolved by Stern in 1924 by some modifications. The Stern model recognized two regions of spatial distribution of ions – the inner region known as the compact or Stern layer and the outer diffuse region as shown in Figure

2.2 (c). He stated that the inner region of ion distribution in the solution is an adsorption process according to Langmuir's adsorption isotherm, and the region beyond this inner layer could be considered as a diffuse region of distributed ionic charge [144]. Stern assumed that the ions have a finite size that includes the annular thickness of their hydration shells and using this assumption, he defined a geometrical limit in the compact region for ion adsorption at the electrode surface. The ions are strongly adsorbed in the Stern layer forming the inner Helmholtz plane (IHP) and the outer layer consists of non-specifically adsorbed counterions, which form the outer Helmholtz plane (OHP) [218]. Therefore the EDL charge density according to the Stern model is a combination of the Helmholtz model of compact double layer exhibiting a capacitance C_H and the Gouy-Chapman model of the diffuse region of double layer having a capacitance C_{diff}. The overall EDL capacitance (C_{dl}) is the total capacitance from the two regions, C_H and C_{diff} and can be expressed by the following equation:

$$\frac{1}{C_{dl}} = \frac{1}{C_H} + \frac{1}{C_{diff}} \tag{2.10}$$

Although the above models give a satisfactory description of the EDL formation and the EDL capacitance at a planar electrode surface, the capacitance is also affected by other factors such as the electric field across the electrode, the size and shape of electrolyte ions, the solvent in which the electrolyte ions are dissolved and the chemical affinity between the adsorbed ions and the electrode surface. For an EDL capacitor, the capacitance is generally considered similar to that of a parallel-plate capacitor and is given by [219]:

$$C = \frac{\varepsilon_r \varepsilon_0 A}{d} \tag{2.11}$$

where ε_r is the dielectric constant of the electrolyte, ε_0 is the permittivity of free space, A is the electrode's specific surface area in contact with the electrolyte and d is the EDL thickness i.e. the distance between the OHP and the electrode surface. However, for electrode materials with variable sized pores, the EDL charge distribution is not similar to that of an infinite planar electrode and depends on various other parameters such as ion transport pathways, mobility of ions into the pores, ohmic resistance of the electrolyte and wettability of pores by the electrolyte. The mobility of ions into the electrode pores is greatly governed by the pore size, which if too small makes the pores inaccessible to the electrolyte ions reducing their

contribution to EDL capacitance [8]. As all the pores are not accessible to the ions, the linear relationship based on equation (2.11) between specific capacitance and specific surface area does not hold in case of porous electrodes. However, there is a general agreement that the presence of mesopores (pore size > 2 nm) can enhance the power performance of a supercapacitor by promoting electrolyte accessibility to the micropore surface where charge storage takes place [220]. For estimating the capacitance of carbon materials depending on the pore size and shape, two different models have been proposed. An electric double-cylinder capacitor model is employed for describing mesoporous carbon electrodes and an electric wire-in-cylinder capacitor model is used for modelling microporous carbon electrodes [221]. In case of mesoporous carbons with cylindrical pores, the capacitance can be calculated using the following equation:

$$C = \frac{\varepsilon_r \varepsilon_0}{b ln\left(\frac{b}{b-d}\right)} A \tag{2.12}$$

where A is electrode's surface area, b is the radius of pore and d is the distance between the ion and the electrode surface. For micropores, the ions are considered to line up in the centre of a cylindrical pore and the capacitance is given by:

$$C = \frac{\varepsilon_r \varepsilon_0}{b ln\left(\frac{b}{a_0}\right)} A \tag{2.13}$$

where a_0 is the effective size of the counterions. However, a sandwich capacitance model has been proposed later for carbon electrodes having a pore shape of slit and not a cylinder [222], which is given by:

$$C_s = \frac{\varepsilon_r \varepsilon_0}{b - a_0} A \tag{2.14}$$

2.2 Origin of pseudocapacitance

Pseudocapacitance is a faradaic charge storage process that arises due to chemical state changes of the electrode material involving transfer of charges (ΔQ) across the interface with a change in potential (ΔV) leading to a proportionality constant, which corresponds to a capacitance, referred to as the pseudocapacitance. The pseudocapacitance is calculated by the following equation [219]:

$$C_{pc} = \frac{\Delta Q}{\Delta V} \tag{2.15}$$

Faradaic redox processes in a pseudocapacitor lead to passage of extent of charge *q*, which occurs due to a thermodynamic change in potential. The redox processes can be defined as:

$$Ox + ne^- \rightleftharpoons Red \tag{2.16}$$

where *n* is the electron transfer number, *Ox* is the oxidized species and *Red* is the reduced species. The thermodynamic change in electrode potential for such redox system is governed by the Nernst equation [41], which can be written as:

$$E = E^0 + \frac{RT}{nF} ln \frac{[Ox]}{[Red]} \tag{2.17}$$

where *E* is the electrode potential, E^0 is the standard electrode potential of the redox couple, *R* is the universal gas constant, *F* is the Faraday constant, *T* is the temperature, and [*Ox*] and [*Red*] represents the concentration of the oxidized and the reduced species, respectively. For a given molar quantity *Q* of reagent, where *Q* = [*Ox*] + [*Red*], equation (2.17) can be written in terms of fractions as:

$$E = E^0 + \frac{RT}{nF} ln \frac{\left[\frac{Ox}{Q}\right]}{\left[\frac{Red}{Q}\right]} \tag{2.18}$$

$$E = E^0 + \frac{RT}{nF} ln \frac{\left[\frac{Ox}{Q}\right]}{\left(1 - \left[\frac{Ox}{Q}\right]\right)} \tag{2.19}$$

Rearranging equation (2.19), we obtain:

$$\frac{\left[\frac{Ox}{Q}\right]}{\left(1 - \left[\frac{Ox}{Q}\right]\right)} = exp\left((E - E^0)\frac{nF}{RT}\right) = exp\left(\Delta E \frac{nF}{RT}\right) \tag{2.20}$$

Differentiating equation (2.20) with respect to Δ*E* gives rise to a formal capacitance, which is given by [144]:

$$\frac{C_{pc}}{Q} = \frac{d}{dE}\left[\frac{Ox}{Q}\right] = \frac{\frac{nF}{RT} exp\left(\Delta E \frac{nF}{RT}\right)}{\left[1 + exp\left(\Delta E \frac{nF}{RT}\right)\right]^2} \tag{2.21}$$

which exhibits a maximum value at [*Ox*] = [*Red*] = ½ (*Q*) and $E = E^0$, where *Q* corresponds to the total charge associated with the oxidation or reduction of the material. The capacitance quantity C_{pc} in equation (2.21) is referred to as pseudocapacitance that arises from the faradaic reactions of equation (2.16).

2.3 Current-voltage characteristics

Low dimensional conducting polymers particularly nanotubes and nanowires exhibit unusual electronic properties due to their disordered structure comprising of randomly oriented polymer chains. These polymer chains consist of ordered chain folding in some regions, while in other regions, the chains are less-ordered. The structure of conducting polymers is therefore inhomogeneous, which is a combination of conducting regions that are separated by small insulating barriers. Such a quasi-one-dimensional disordered system is observed to exhibit non-linear current-voltage (I-V) characteristics because of the mixed crystalline and amorphous regions in their structure. The non-linear I-V characteristics of conducting polymers have been described using the Kaiser model, which takes advantage of the FIT mechanism. The FIT conduction mechanism proposed by Sheng [223], describes electron transport across insulating barriers, which can be controlled by the voltage variations in the conducting pathways. The average current density through a barrier upon application of a field E_a across it can be written as [224]:

$$j(E_a) = \int_{-\infty}^{\infty} dE_T \, j(E_a + E_T) P(E_T) \tag{2.22}$$

where $P(E_T)$ is the probability that the fluctuating field across the junction exhibits the value E_T (which may be in either direction). The expression for tunnelling current $j(E)$ for a total field $E_b = (E_a + E_T)$ across the barrier can be written as [223]:

$$j(E_b) = \frac{me}{8\pi^2 \hbar^3} \int_{-\infty}^{\infty} d\varepsilon \, D(\varepsilon, E_b) \, \boldsymbol{\Theta}(\varepsilon, E_b) \tag{2.23}$$

where m and ε are the mass and energy of charge carrier, respectively. $D(\varepsilon, E_b)$ represents the barrier transmission factor given by approximation of the usual exponential WKB expression with $D(\varepsilon, E_b) = 1$ when the energy ε is greater than that of the tunnelling barrier, and $\boldsymbol{\Theta}(\varepsilon, E_b)$ indicates the appropriate "supply function" governed by the Fermi factors on each side of the barrier. Considering the current fluctuation-assisted tunnelling through conducting regions and thermal activation across the barriers, Kaiser et al. put forward a generic expression based on the structural features of quasi one-dimensional disordered materials and the FIT model, which can describe the non-linear I-V characteristics in quasi one-dimensional systems [225]:

$$G = \frac{I}{V} = \frac{G_0 \, exp(^V/_{V_0})}{1 + h[exp(^V/_{V_0}) - 1]} \tag{2.24}$$

where G_0 implies the temperature-dependent low-field conductance (for V tends to zero) and V_0 (depends strongly on barrier energy) measures the voltage scale factor that yields an exponential increase in conductance with increase in V. As the field increases upto the point that the Fermi level difference on either side of the barrier is comparable to the barrier energy, saturation in conductance will be obtained at a value G_h which measures larger conductance in the absence of barriers. The parameter $h = {}^{G_0}/_{G_h}$ (where $h < 1$) exhibits a decrease in the G value below the exponential increase at higher voltages V.

The dc conductivity for a film of thickness *t* can be calculated using four-probe method from the following equations:

$$\text{Resistivity}\,(\rho, \text{ohm} - \text{cm}) = \frac{\pi t}{\ln 2}\left(\frac{V}{I}\right) \tag{2.25}$$

$$\text{Conductivity}(\sigma, \text{S cm}^{-1}) = \frac{1}{\rho} \tag{2.26}$$

where *I* is the source current through the outer two probes and *V* is the measured voltage across the inner two probes.

2.4 Parameters evaluating the performance of supercapacitors

The performance of a supercapacitor is evaluated in terms of various factors that determine its charge storage efficiency, which are described below:

(i) Specific capacitance: The specific capacitance refers to measured capacitance of an electrode by current vs. voltage (I-V) plot or voltage vs. time (V-T) plot using the following equation:

$$C_{sp}\left(\frac{F}{g}\right) = \frac{I}{\left(\frac{dV}{dt}\right)w} \tag{2.27}$$

where *I* is the current in ampere, (*dV/dt*) is the rate of change of voltage in Volt/sec and *w* corresponds to the mass (g) or area (cm^2) or volume (cm^3) of the electrode. If *w* is the electrode's mass, then C_{sp} is called gravimetric capacitance, for *w* = area, it is areal capacitance and for volume, C_{sp} is termed as volumetric capacitance [44]. The specific capacitance can be measured using different electrochemical

configurations such as two-electrode cell and three-electrode cell for which the calculation of specific capacitance is different. For a two-electrode system, the capacitance is given by, C_{2E} = ½ C and the gravimetric specific capacitance become:

$$C_{sp} = \frac{C_{2E}}{2m} = \frac{C}{4m} \tag{2.28}$$

where m is the mass of each individual electrode. For a three-electrode configuration, the capacitance is given by, C_{3E} = C and the gravimetric specific capacitance is measured as:

$$C_{sp} = \frac{C_{3E}}{m} = \frac{C}{m} \tag{2.29}$$

The capacitance of an electrode highly depends on the electrode material characteristics and the electrolyte.

(ii) Energy density and power density: In evaluating the performance of an electrode material, the energy density and power density are crucial factors. Energy density is the amount of energy stored per unit weight of the electrode, while power density determines the rate at which the electrode could be charged or discharged. When an electrode is charged or discharged within a potential range 'ΔV', the energy density (E) and power density (P) of the electrode can be expressed as [226]:

$$E(Wh/kg) = \frac{1}{2} C_{sp} (\Delta V)^2 \tag{2.30}$$

$$P(W/kg) = \frac{E}{\Delta t_d} \tag{2.31}$$

where C_{sp} is the gravimetric specific capacitance of the electrode and Δt_d is the discharge time. In order to improve the energy density and power density of an electrode, its C_{sp} and ΔV need to be increased.

(iii) Equivalent series resistance: If a sinusoidal ac is applied to an ideal capacitor, the output voltage should be out of phase by 90°, independent of frequency. However, in case of supercapacitors, the output voltage is out of phase by less than 90° implying that an equivalent series ohmic resistor is coupled. This ohmic component is termed as equivalent series resistance (ESR), which is a real series resistance in supercapacitors and affects their power density. An increase in ESR limits the charge-discharge rate of an electrode leading to low power density. Various types of resistances contribute to ESR that includes ionic resistance of the electrolyte, intrinsic resistance of the electrode material, contact resistance between

the electrode and current collector and mass transfer resistance of the electrolyte ions [227]. Utilizing electrolytes with high ionic conductivity can reduce the ESR and improve the power density.

(iv) Coulombic efficiency: In supercapacitor, the coulombic efficiency (η) is defined as the ratio of amount of charges extracted from the electrode during discharge to the amount of charges stored in the electrode during charging. It is calculated by the ratio of discharging time to the charging time when the charge-discharge current densities are equal, which can be written as [228]:

$$\eta = \frac{\Delta t_d}{\Delta t_c} \times 100\% \tag{2.32}$$

where Δt_d and Δt_c are the discharging and the charging times. The coulombic efficiency is affected by several factors such as electrolyte side reactions, impurity in electrolyte and structural instability of electrode material that causes electron loss during discharging and reduces η.

(v) Cycle life: The investigation of cycle life is necessary to evaluate the stability of the electrode i.e. the number of charge-discharge cycles that can be sustained by an electrode during its lifetime [44]. It is an estimate of the expected working lifetime of an electrode and is determined by calculating the capacitive retention of the electrode from current vs. voltage (I-V) or voltage vs. time (V-T) measurements for repeated number of cycles. The cycle life is dependent on various factors such as electrode material, electrolyte, operating voltage window, charge-discharge rate and temperature.

2.5 Cyclic voltammetry

Cyclic voltammetry (CV) is a widely used technique for studying the electrochemical properties of supercapacitor electrodes including electrochemical redox processes, charge transfer kinetics and charge storage mechanism. From CV, qualitative information such as capacitance, conductivity, reversibility, polarization and the position of oxidation and reduction peaks could be obtained. The principle of this technique is to apply a time-dependent triangular voltage waveform to the working electrode and the resulting current is measured. A linear voltage sweep is applied between time t_0 and t_1 until it reaches a final voltage V_2. The scan is then reversed and the potential moves from t_1 to t_2 and reaches V_1 at the same scan rate.

The rate at which the potentials are scanned is known as the scan rate. The potential-time plot can be expressed as [229]:

$$V(t) = V_1 + \nu t \qquad for\ 0 \leq t \leq t_1 \tag{2.33}$$
$$V(t) = V_1 + \nu t_\lambda - \nu t \qquad for\ t_1 \leq t$$

where V_1 is the initial potential of the scan, ν is the scan rate in mV s^{-1} and t_1 is the switching time of the triangular waveform as shown in Figure 2.3. The output of the CV is a graph of the measured current passing through the working electrode with respect to the applied voltage, which is an enclosed curve referred to as cyclic voltammogram.

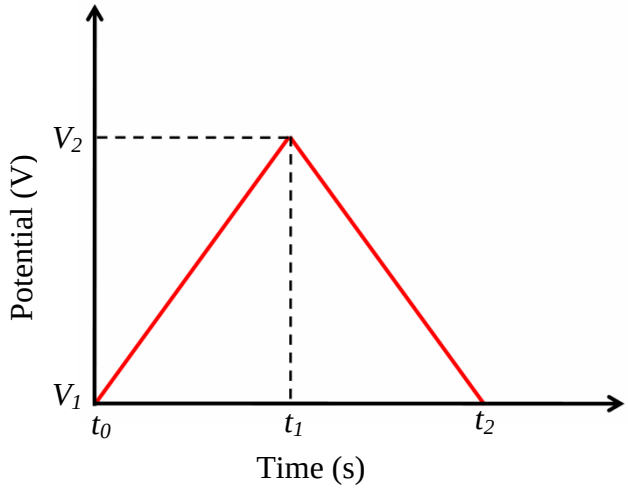

Figure 2.3: *Triangular voltage waveform applied to the working electrode.*

The shape of the CV curve is an indication of the charge storage mechanism in the electrode. The area under the cyclic voltammogram is an estimate of the total amount of charge stored by the electrode from which the capacitance can be calculated using the following equation [230]:

$$C = \frac{Q}{|V_2 - V_1|} \tag{2.34}$$

The total charge Q can be obtained by integrating the whole area under the CV from V_1 to V_2 recorded at a voltage scanning rate $\nu = dV/dt$ and is given by [144]:

$$Q = \int_{V_1}^{V_2} I(V)dt \tag{2.35}$$

where I is the measured current density within potential limits V_1 and V_2. Substituting $dt = dV/\nu$, we obtain:

$$Q = \frac{\int_{V_1}^{V_2} I(V)dV}{\nu} \tag{2.36}$$

where $\int_{V_1}^{V_2} I(V)dV$ is the enclosed CV area. Substituting the value of Q in equation (2.34), the capacitance can be written as:

$$C = \frac{\int_{V_1}^{V_2} I(V)dV}{v|V_2 - V_1|} \tag{2.37}$$

The specific capacitance is then obtained as:

$$C_{sp} = \frac{1}{2}\left(\frac{\int_{V_1}^{V_2} I(V)dV}{mv\Delta V}\right) \tag{2.38}$$

where m is the mass of the electrode material, v is the potential scan rate and ΔV is the operating potential window. Since a CV cycle contains both charging and discharging processes, the entire area should be divided by two to obtain the specific capacitance. The cycle life of supercapacitor electrodes can also be determined from CV by observing the changes in specific capacitance over many cycles. With prolonged CV cycles, the capacitance of the electrode will decrease while the ESR will increase leading to a decrease in both energy and power densities, which can be calculated according to the number of CV cycles. The measured difference of specific capacitance between the first cycle and the last cycle gives an estimate of the cycle life of the electrode.

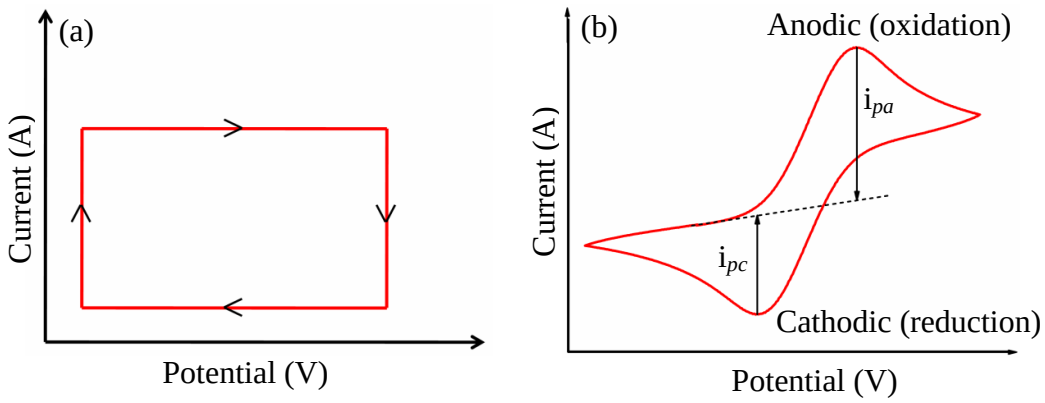

Figure 2.4: *Representation of CV of (a) ideal EDL capacitor, and (b) pseudocapacitor.*

The CV of an ideal EDL capacitor is rectangular as shown in Figure 2.4 (a). However, experimentally obtained CV's show deviations from rectangular shape due to various resistances related to electrode and electrolyte, porosity of electrode etc. Pseudocapacitive materials exhibit non-rectangular CV's with intense peaks due to

faradaic oxidation and reduction reactions on the electrode surface as shown in Figure 2.4 (b). The upper half of the CV represents oxidation and the lower half indicates reduction with the current maxima referred to as the anodic (i_{pa}) and cathodic peak currents (i_{pc}), respectively. The scan rate and the number of CV cycles can vary the specific capacitance. The specific capacitance decreases with increasing scan rate [231]. At low scan rates, the electrolyte ions have sufficient time to penetrate the pores of the electrode, whereas at higher scan rates, the ions accumulate only on the electrode surface. Moreover, the faradaic reactions occurring on the electrode surface are not able to follow the fast change in electrode potential resulting in incomplete reactions and low current output, which decrease the capacitance at high scan rates.

2.6 Galvanostatic charge-discharge

Galvanostatic charge-discharge (GCD) is another technique for studying the electrochemical behavior of supercapacitor electrodes, which is accepted as a standard method to calculate the specific capacitance.

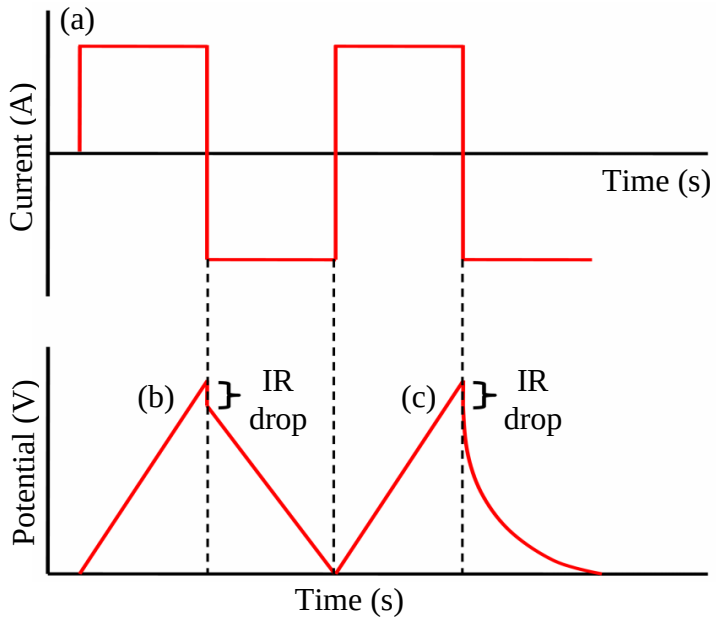

Figure 2.5: *(a) Constant current reversal cyclic chronopotentiometry; Representation of GCD curve for (b) EDL capacitor, and (c) pseudocapacitor.*

This method is also known as chronopotentiometry, where a constant current pulse is applied to the working electrode and the resulting potential is measured with respect

to a reference electrode as a function of time as depicted in Figure 2.5 (a). The applied current pulse is reversed periodically, which charge and discharge the electrode within a fixed voltage range in a cyclic manner. The output of the GCD measurement gives a linear variation of voltage with time, which is given by [232]:

$$V(t) = IR + \frac{t}{C}I \tag{2.39}$$

where *V(t)* is the voltage as a function of time, *R* is the resistance, *I* is the applied constant current and *C* is the capacitance. From the slope of the discharge curve, the capacitance of the electrode can be evaluated using the following equation:

$$C = \frac{dQ}{dV} = \frac{Idt}{dV} = \frac{I\Delta t_d}{\Delta V} \tag{2.40}$$

The specific capacitance is then obtained as [233]:

$$C_{sp} = \frac{I\Delta t_d}{m\Delta V} \tag{2.41}$$

where *m* is the mass of the electrode material, Δt_d is the discharge time and ΔV is the discharge potential. The specific capacitance can be calculated at different current densities, which decreases with an increase in applied current density. EDL electrodes exhibit a linear charge-discharge profile, while pseudocapacitive materials deviate from linearity as depicted in Figures 2.5 (b) and (c). A sudden drop in voltage (IR drop) in the initial portion of the discharge curve is observed, which is due to ESR of the electrode and can be deduced from the equation [232]:

$$R = \frac{V_{drop}}{I} \tag{2.42}$$

This voltage drop should be excluded from the discharge potential (ΔV) that is used for calculating the specific capacitance. The energy and power densities can be calculated using equations (2.30) and (2.31) given in section 2.4.

2.7 Electrochemical impedance spectroscopy

Electrochemical impedance spectroscopy (EIS) is an effective technique to study different types of internal resistances associated with the electrode and electrolyte of an electrochemical system. The interfacial electrochemical processes of electrode-electrolyte are studied using EIS in terms of parameters such as ESR, charge transfer resistance, interfacial capacitance and diffusion resistance. In EIS, ac sinusoidal potential of small amplitude is applied in a wide range of frequencies and the current

response is measured to obtain the impedance of the system. This measurement covers a large timescale in the range of microseconds to hours, which separates different electrochemical processes according to their own time constant and reveals underlying interfacial phenomena. As the signal is small enough, there exists a linear relation between the current and voltage at each pulse i.e. the current response will be a sinusoid at the same frequency but shifted in phase. The applied sinusoidal potential can be expressed as [234]:

$$E(t) = E_0 exp(j\omega t) \tag{2.43}$$

where E_0 is the potential amplitude, $\omega = 2\pi f$ is the applied frequency, $j = \sqrt{-1}$ and t is the time.

The current response is obtained as:

$$I(t) = I_0 exp[j(\omega t - \varphi)] \tag{2.44}$$

where I_0 is the current amplitude and φ is the phase angle.

The impedance can then be represented as a complex number:

$$Z(\omega) = \frac{E(t)}{I(t)} = Z_0 exp(j\varphi) = Z_0(cos\varphi + jsin\varphi) \tag{2.45}$$

$$\Longrightarrow Z(\omega) = Z^{'} - jZ^{''} \tag{2.46}$$

The magnitude of Z can be written as:

$$|Z(\omega)| = \sqrt{(Z^{'})^2 + (Z^{''})^2} \tag{2.47}$$

and the phase angle as:

$$\varphi = tan^{-1}\left(\frac{Z^{''}}{Z^{'}}\right) \tag{2.48}$$

where Z' and Z'' are the real and imaginary parts of impedance.

When the real part is plotted on the X-axis and the imaginary part of impedance is plotted on the Y-axis, a complex plane diagram is obtained, which is known as Nyquist plot and is depicted in Figure 2.6. The Nyquist plot represents the variation of impedance of the electrochemical system with frequency (ω) where each point in the plot is the impedance at a particular frequency. In this plot, the Y-axis is negative and the frequency increases from the right to the left side of the plot. The magnitude of impedance can be expressed as a vector of length $|Z|$ and the angle between this vector and the X-axis gives the phase angle φ.

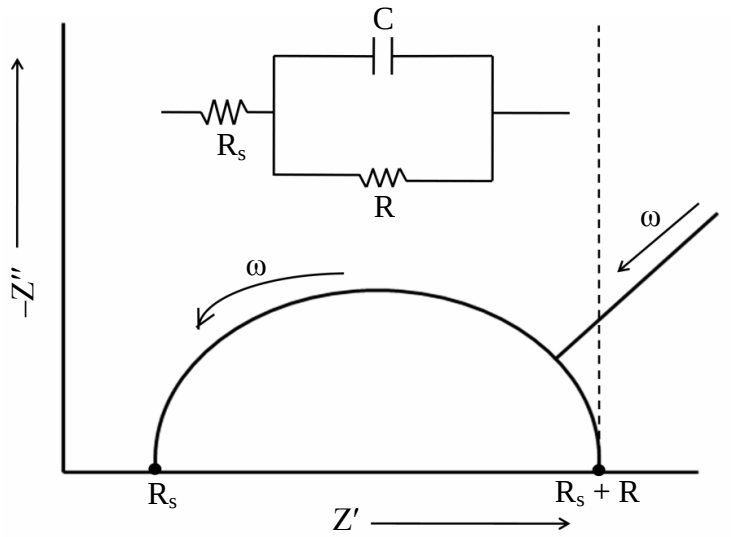

Figure 2.6: *Typical shape of Nyquist plot. Inset shows the equivalent circuit for the Nyquist plot comprising of a semicircle.*

The Nyquist plot is analyzed based on a Randles equivalent circuit, which represents the various electrochemical processes occurring within the system in terms of resistors, capacitors, inductors and their series and parallel combinations [235]. The Randles equivalent circuit for the Nyquist plot comprising of a semicircle is the characteristic of a single time constant '*RC*' i.e. a resistance (*R*) and a capacitance (*C*) in parallel as shown in the inset of Figure 2.6. The total complex impedance for the equivalent circuit can be written as:

$$\frac{1}{Z} = \frac{1}{R} + \frac{1}{(1/j\omega C)} \tag{2.49}$$

$$\Longrightarrow Z = \frac{R}{1 + j\omega RC} \tag{2.50}$$

The real and imaginary parts of *Z* can be obtained from equation (2.50) as:

$$Z^{'} = \frac{R}{1 + \omega^2 C^2 R^2} \tag{2.51}$$

$$Z^{''} = \frac{-R^2 \omega C}{1 + \omega^2 C^2 R^2} = -Z^{'} \omega RC \tag{2.52}$$

Eliminating ωRC from equations (2.51) and (2.52) yields

$$Z^{''\,2} + Z^{'\,2} - RZ^{'} = 0 \tag{2.53}$$

$$\Longrightarrow \left(Z^{'} - \frac{R}{2}\right)^2 + Z^{''\,2} = \left(\frac{R}{2}\right)^2 \tag{2.54}$$

which is the equation of a circle of radius *R*/2 with its centre at (*R*/2,0).

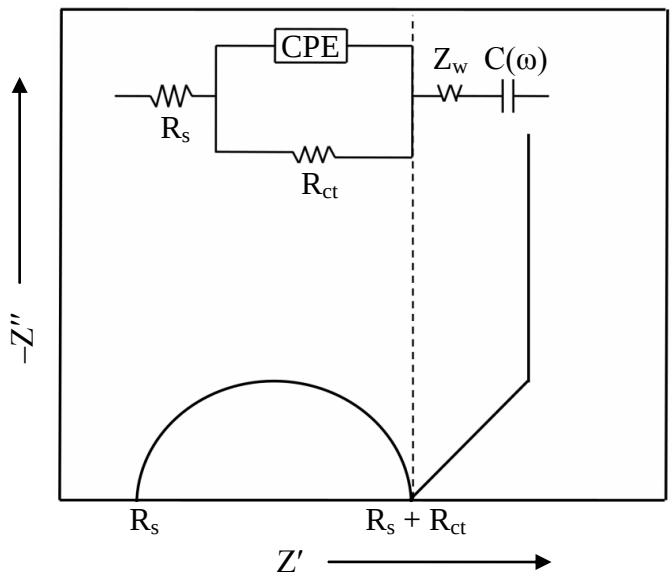

Figure 2.7: *Impedance behavior of a supercapacitor cell. Inset shows the corresponding equivalent circuit for the Nyquist plot.*

The impedance behavior of a supercapacitor cell consisting of an electrode in contact with an electrolyte and applied to small ac signal perturbation can be described by the Nyquist plot in Figure 2.7 and the corresponding equivalent circuit as shown in the inset [236]. At high frequencies, the cell behavior is represented by charge transfer resistance (R_{ct}) connected in parallel with interfacial capacitance (*CPE*), which is combined in series with equivalent series resistance (R_s). The low frequency behavior is described by the Warburg impedance (Z_W) and the supercapacitor cell capacitance ($C(\omega)$) respectively. R_s arises from the combined resistance that includes the ionic resistance of electrolyte, intrinsic resistance of the electrode material and contact resistance between the electrode and current collector and is obtained from the x-intercept of the Nyquist plot. The diameter of the semicircle in Nyquist plot is associated with the charge transfer resistance (R_{ct}) and interfacial capacitance (*CPE*) across the electrode-electrolyte interface. The interfacial capacitance is expressed in terms of constant phase element (*CPE*), which is attributed to variation in capacitance contribution with electrode position due to microscopic irregularities at the electrode-electrolyte interface. The Warburg impedance (Z_W) represents the impedance of diffusional transport of electrolyte ions into the electrode, which gives rise to a 45° straight line in the mid-frequency region [237]. The ($C(\omega)$) is the double layer capacitance built up due to charge accumulation at the electrode-electrolyte interface, which appears as a vertical spike

almost parallel to *Z*'' at low frequencies in the Nyquist plot and is a signature of pure capacitive behavior.

2.8 The Brunauer-Emmett-Teller (BET) theory

The Brunauer-Emmett-Teller (BET) theory is the most popular approach for the measurement of specific surface area by physical adsorption of gas molecules. This theory utilizes probing gases that do not react chemically with material surfaces to estimate the specific surface area. Nitrogen is employed as the standard gaseous adsorbate for BET surface area analysis. The adsorption of N_2 gas molecules takes place on the solid surface, which is reversible due to weak van der Waals bonding between them, therefore the experiment is known as N_2 adsorption-desorption measurements. The specific surface area of a solid is measured by evaluating the number of molecules adsorbed on the surface and the effective cross-sectional area covered by each adsorbed molecule on the solid surface. The surface area is then calculated from the product of the number of molecules and the effective cross-sectional area of an adsorbate molecule. Langmuir proposed the adsorption isotherm with the assumption that a solid surface can be represented as an array of adsorption sites and dynamic equilibrium exists between the adsorbed gaseous molecules and free gaseous molecules. Based on this theory, Langmuir derived the equation for monolayer molecular adsorption using the kinetic theory of gases [238], which gives the relation between the number of active sites of the surface undergoing adsorption and pressure, given by:

$$\frac{n}{n_m} = \frac{v}{v_m} = \frac{KP}{1 + KP} \tag{2.55}$$

where n is the number of adsorbates adsorbed, n_m is the number of adsorbates required to complete one monolayer, v/v_m is the volume adsorbed relative to the volume adsorbed in a complete monolayer, P is the pressure and K is the equilibrium constant for distribution of adsorbate between the surface and the gas phase. However, this theory is applicable only under conditions of low pressure. The Langmuir's kinetic theory was extended by Brunauer, Emmett and Teller on the assumption that multilayer adsorption would occur under the condition of high pressure and low temperature due to decrease of thermal energy of gaseous molecules which will increase the availability of molecules per unit surface area.

Using the assumption of multilayer adsorption theory, the BET equation is derived as [239]:

$$\frac{1}{v[(p_0/p)-1]} = \frac{c-1}{v_m c}\left(\frac{p}{p_0}\right) + \frac{1}{v_m c} \tag{2.56}$$

where p and p_0 are the equilibrium and saturation vapour pressure of adsorbates, v is the adsorbed gas quantity, v_m is the monolayer adsorbed gas quantity and c is the BET constant given by:

$$c = exp\left(\frac{E_1 - E_L}{RT}\right) \tag{2.57}$$

where $(E_1 - E_L)$ is the net heat of adsorption. The calculation of specific surface area from BET theory is a straightforward application of the BET equation (2.56), which can be plotted as a straight line with $1/v[(p_0/p) - 1]$ on the y-axis and p/p_0 on the x-axis. This plot is called a BET plot. The linear relationship of this equation is maintained only in the range of $0.05 < p/p_0 < 0.35$. From the slope S and the y-intercept I of the line, the monolayer adsorbed gas quantity v_m and the BET constant c can be calculated using the following equations:

$$v_m = \frac{1}{S+I} \tag{2.58}$$

$$c = 1 + \frac{S}{I} \tag{2.59}$$

The total surface area of the material is given by:

$$S_{total} = \frac{v_m N s}{V} \tag{2.60}$$

where N is Avogadro's number, s is the adsorption cross-section of the adsorbing species and V is the molar volume of the adsorbate gas. The BET specific surface area is then obtained as:

$$S_{BET} = \frac{S_{total}}{M} \tag{2.61}$$

where M is the mass of the solid material.

Depending on the pore structure of different materials, the adsorption-desorption isotherms are classified into six types [240], which are presented in Figure 2.8. Type I isotherms are obtained for microporous materials as micropore filling and high uptakes occur at relatively low pressures due to the narrow pore width and high adsorption potential. Type II sorption isotherms indicate non-porous or macroporous materials, where unrestricted monolayer-multilayer adsorption occurs. The point B is the stage at which monolayer coverage is complete and

multilayer adsorption starts. Type III isotherms are observed when the attractive adsorbate-adsorbent interactions are relatively weak and the adsorbate-adsorbate interactions come into play. Type IV and V isotherms with hysteresis loop are indicative of occurrence of pore condensation in mesoporous materials. Type VI isotherms are specially observed when multilayer adsorption occurs on a uniform non-porous surface.

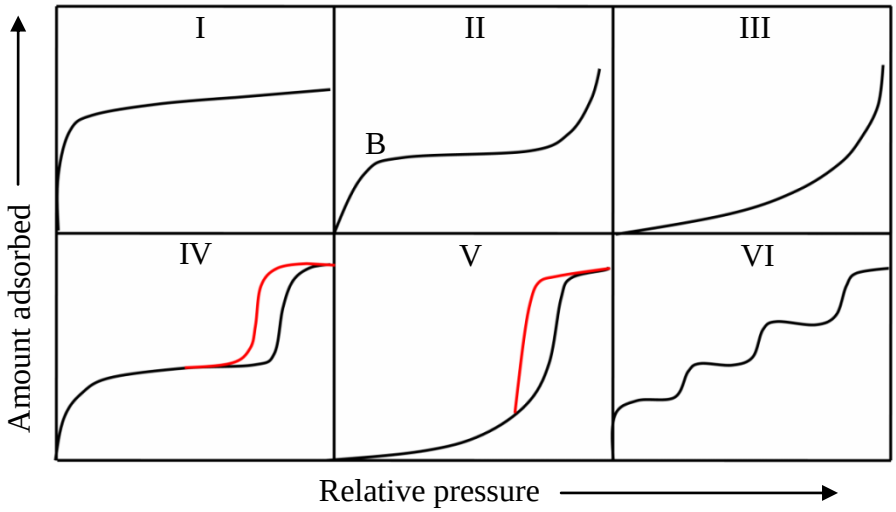

Figure 2.8: *Schematic representation of different types of nitrogen adsorption-desorption isotherms.*

2.9 Determination of pore size using Barrett, Joyner and Halenda (BJH) method

The Barrett, Joyner and Halenda (BJH) method serves as the basis for pore size determination of materials. The BJH method is the modification of Kelvin's equation, which is based on the Wheeler's theory that condensation occurs in pores when a critical relative pressure is reached corresponding to the Kelvin radius r_k. The Kelvin equation gives the relation between the equilibrium vapor pressure exerted from the curved meniscus of the pore liquid (P) and the equilibrium pressure of the same liquid on a planar surface (P_0). For pore of cylindrical shape, the Kelvin equation is expressed as [241]:

$$\ln\frac{P}{P_0} = \frac{-2\gamma\overline{V}}{rRT} \tag{2.62}$$

where γ is the surface tension of the liquid, $\overline{V}$ is the molar volume of the condensed liquid contained in a narrow pore of radius r, R is the gas constant and T is the

temperature. For nitrogen as adsorbate at its boiling temperature (77 K), the Kelvin equation becomes [242]:

$$r_k = \frac{4.15}{\log(P_0/P)} \tag{2.63}$$

where r_k is known as the Kelvin radius into which condensation occurs at the required relative pressure. This radius does not give the actual pore radius as some adsorption already occurrs on the pore wall prior to condensation, leaving a centre core of radius r_k. The actual pore radius is given by:

$$r_p = r_k + l_c \tag{2.64}$$

where l_c is the thickness of the adsorbed film when condensation or evaporation occurs in a given pore size. The depth of the adsorbed multilayer film is expressed in the form of statistical thickness *t*, which for liquid nitrogen can be written as:

$$t = 3.54\left(\frac{5}{\ln P_0/P}\right)^{1/3} \tag{2.65}$$

The change in adsorbed volume of liquid nitrogen ΔV_{liq} is determined from ΔV_{gas} by calculating the number of moles of gas and multiplying by the molar volume of nitrogen:

$$\Delta V_{liq} = \frac{\Delta V_{gas}}{22.4 \times 10^3} \times 34.6 = \Delta V_{gas}\,(1.54 \times 10^{-3}) \tag{2.66}$$

where ΔV_{gas} is the corresponding change in adsorbed volume of gas. The actual pore volume is then calculated from ΔV_{liq} using the following equation:

$$V_p = \left(\frac{\overline{r_p}}{\overline{r_k}}\right)^2 \left[\Delta V_{liq} - (\Delta t \Sigma S \times 10^{-4})\right] \tag{2.67}$$

where *S* is the surface area of the pore walls and is given by [243]:

$$S = \frac{2V_p}{\overline{r_p}} \times 10^4 \tag{2.68}$$

The pore size distribution curve is obtained by plotting $\overline{r_p}$ on the x-axis and ($V_p/\Delta r_p$) on the y-axis.

If the adsorption isotherm exhibits a distinct plateau as shown in type IV and V isotherms in Figure 2.8, the total pore volume can be obtained from a single point adsorption at a relative pressure (P/P_0) of 0.95. The value of P/P_0 = 0.95 is chosen because the relative pressure value should be located after the pore condensation stage. In this case, the adsorbed amount gives the adsorption capacity and the total pore volume is determined by converting the amount adsorbed into liquid volume

with the assumption that the density of the adsorbate is equal to the bulk liquid density at saturation. The pore volume is calculated using the equation [242]:

$$V_p = \frac{W_a}{\rho_l} \tag{2.69}$$

where W_a is the adsorbed amount in grams and ρ_l is the liquid density.

2.10 Determination of surface energy using contact angle measurements

The atoms at the surface of a solid or liquid material experience different environment as compared to that of its bulk. The difference arises due to the variation in the co-ordination number of the atoms. The atoms in the bulk are surrounded by neighbouring similar atoms from all sides, which results in a net force of zero on the atoms and a lower energy state. However, the atoms at the surface do not experience force from all directions and therefore experience a net inward force. Moreover, the various external forces from the environment act only on the surface atoms and therefore they are in a higher energy state as compared to that of the bulk atoms. This energy difference between the atoms at the surface and bulk atoms is expressed as surface tension (or surface free energy), γ. The surface free energy is a crucial parameter that evaluates the wettability and adhesion properties of solid materials. Wettability implies the degree to which a liquid spreads on a solid surface when it comes into contact with it. Lower values of contact angle indicate the spreading of a liquid on the solid surface while high contact angle values imply poor spreading. If the contact angle value is less than 90°, then the liquid wets the surface while contact angles greater than 90° indicate that the liquid does not wet the solid surface. Zero contact angle represents complete wetting of the solid surface by the liquid. Contact angle measurement is considered as one of the simplest and reliable method for determination of surface energy and the degree of interaction between a solid material and a liquid at the lowest equilibrium distance [244]. The surface energy of a polymeric material can be split into polar component (γ_S^p) and apolar or dispersive component (γ_S^d). Several models such as Owens, Wendt, Rabel and Kaelble (OWRK) method, Zisman method, Van Oss-Chaudhury-Good method etc. have been used for calculation of surface energy of solid surface by using the contact angle values of different measuring liquids [245, 246]. In the present work, the

OWRK method has been employed to calculate the surface free energy, which uses water (polar) and diiodomethane (apolar) as the measuring liquids.

The OWRK method is a model based calculation of surface energy of a solid surface using two standard testing liquids and is a modification of Fowkes theory. According to Fowkes theory, the surface energy of a solid and liquid is a sum of independent components, associated with various interfacial interactions:

$$\gamma_s = \gamma_s^d + \gamma_s^p + \gamma_s^h + \gamma_s^i + \gamma_s^{ab} + \dots\dots\dots \quad (2.70)$$

where superscripts *d, p, h, i* and *ab* denote the dispersion force, polar force, hydrogen bonding force, induction force and acid-base force, respectively. The Fowkes theory considered that the dispersion component is connected with London interactions arising from electron-dipole fluctuations. Owen and Wendt modified the Fowkes theory by assuming the sum of components on the right-hand side of equation (2.70) except γ_s^d as polar interaction (γ_s^p) [247]. Therefore, the following relation was derived:

$$\gamma_{SL} = \gamma_S + \gamma_L - 2\sqrt{\gamma_S^d \gamma_L^d} - 2\sqrt{\gamma_S^p \gamma_L^p} \quad (2.71)$$

where γ_S is the surface free energy of the solid, γ_L is the surface free energy of the measuring liquid and γ_{SL} is the surface free energy of the solid-liquid interface. The terms γ_S^d, γ_S^P, γ_L^d and γ_L^p denote the dispersive and polar components of surface energy of the solid and liquid, respectively.

Now, the equilibrium at the three phase contact of solid, liquid and gas is described by the well known Young's equation, which is given by

$$\gamma_S = \gamma_{SL} + \gamma_L \cos\theta \quad (2.72)$$

where θ is the contact angle made by the testing liquid with the solid surface [248]. Combining equation (2.71) with (2.72), we obtain:

$$\sqrt{\gamma_S^d \gamma_L^d} + \sqrt{\gamma_S^p \gamma_L^p} = 0.5\gamma_L(1 + \cos\theta) \quad (2.73)$$

Equation (2.73) is known as OWRK equation by which the polar (γ_S^p) and dispersive (γ_S^d) components of surface energy of a solid surface can be calculated using the contact angle values of two measuring liquids, one polar and one apolar.

2.11 Theories governing the interaction of swift heavy ions with solid target material

Swift heavy ion (SHI) irradiation is a unique tool to modify the properties of materials in a controlled manner for a variety of applications. The primary factor that decides the ion beam induced material modification is the interaction mechanism of the incident ion with the host material. SHI transfer energy through electronic excitation and ionization of the target material, which is about two orders of magnitude higher than the nuclear energy loss (discussed in section 1.8 of Chapter 1) [200]. The mechanism of energy transfer from the incoming energetic SHI to the solid target material has been explained by two theoretical models: (a) Coulomb explosion model, and (b) Thermal spike model, which are briefly discussed below:

(a) Coulomb explosion model: When energetic SHI pass through a material, positively charged target ions are produced along the ion path due to SHI induced electronic excitation and ionization. These positive ions are mutually repulsive and form a long positively charged cylinder within a time interval of 10^{-14} s. As the conduction electrons of the target material are unable to respond within a time interval of 10^{-14} s, charge neutrality could not be established and the positively charged cylinder explodes radially due to conversion of electrostatic energy to coherent radial atomic movements under Coulomb forces until the ions are screened by conduction electrons [203]. This results in cylindrical shock waves along the ion trajectory of diameter less than 10 nm that produces various modifications in the target material such as phase changes, point and columnar defects, carbonization, defect annealing, formation of cylindrical ion tracks etc. This is known as Coulomb explosion model, which explains the mechanism of energy transfer from the electronic energy deposition of incident SHI into atomic motion of the target material [249]. The formation of ion tracks in Coulomb explosion model is governed by some crucial features [250] as given below:

(i) Formation of ion tracks in the target material is possible when the local electrostatic stress generated by SHI is greater than the mechanical strength of the target material, which can be written as:

$$\frac{n^2 e^2}{\epsilon {a_0}^4} > \frac{1}{10} E \tag{2.74}$$

$$\Rightarrow n^2 > \frac{E\epsilon {a_0}^4}{10e^2} \tag{2.75}$$

where, ϵ is the dielectric constant, a_0 is the average atomic spacing, n is the average ionization per atom, e is the electronic charge and E is the Young's modulus of the target material. Equation (2.75) indicates that formation of tracks is easier in materials with low dielectric constant, less mechanical strength and close inter-atomic distance.

(ii) Another requirement for track formation is that the availability of free electrons in the target material must be lower than the excited electrons by SHI along the cylindrical ionized track so that they cannot neutralize the positively charged ions within a time scale of < 10^{-13} s. This condition is given by the following equation:

$$n_n < \frac{en_a}{a_0\mu_n\pi k_B T t} \tag{2.76}$$

where n_n is the number of free electrons, n_a is the number of ionizations per atomic plane, k_B is the Boltzmann constant, μ_n is the electron mobility, t is the diffusion time and T is the temperature.

(iii) The mobility of holes created along the ion track core due to SHI induced ionization must be lower to allow the formation of tracks.

(b) Thermal spike model: According to the thermal spike model, the energetic SHI passing through the material excites the electronic subsystem of the target material by inelastic collisions. The excited electrons reach a thermodynamic equilibrium within a time period of 10^{-15} s via electron-electron interaction. The kinetic energy of the electrons is then transmitted to the lattice by electron-phonon interaction in 10^{-13}-10^{-10} s in a way efficient enough to increase the local lattice temperature above the melting point of the material [251]. This temperature increase generates a localized heating of the atomic system of the target material along the ion trajectory of nanometric dimension, which is known as the thermal spike and lasts for a few picoseconds. The temperature increase is then followed by a rapid quenching of the order of 10^{13}-10^{14} K/s, which results in different structural and morphological changes in the host material when the melt solidifies. This is known as the thermal spike model that describes the transport of energy from SHI to the target material through electron-phonon coupling [252]. The energy transport from SHI to the electronic and lattice subsystems and between the two subsystems is described by two coupled Fourier equations [253] as follows:

$$C_e T_e \frac{\partial T_e}{\partial t} = \frac{1}{r}\frac{\partial}{\partial r}\left[rK_e(T_e)\frac{\partial T_e}{\partial r}\right] - G(T_e - T_a) + A(r,t) \quad (2.77)$$

$$C_a T_a \frac{\partial T_a}{\partial t} = \frac{1}{r}\frac{\partial}{\partial r}\left[rK_a(T_a)\frac{\partial T_a}{\partial r}\right] + G(T_e - T_a) \quad (2.78)$$

where *K*, *T* and *C* are the thermal conductivity, temperature and the volume specific heat capacity, respectively. The radial distance from the ion trajectory and the time are denoted by *r* and *t*, respectively. The electron-phonon interaction is described by the term $G(T_e - T_a)$, where *G* is the coupling constant and $(T_e - T_a)$ is the temperature diffeence between the electronic and lattice subsystems. $A(r,t)$ represents the energy transfer of the projectile ions to the target electrons, which is described by a Gaussian time distribution and a radial energy distribution of secondary electrons according to Waligorski et al. [254].